PAPER • OPEN ACCESS

# Conductive emulsions with selective filler distribution as volume exclusion strategy in electrofluids

Journal of Physics: Materials



OPEN ACCESS

RECEIVED
1 August 2025

REVISED
7 January 2026

ACCEPTED FOR PUBLICATION
27 January 2026

PUBLISHED
10 February 2026



PAPER

# Conductive emulsions with selective filler distribution as volume exclusion strategy in electrofluids

**Dominik S Schmidt**[1], **Dominik Perius**[1] and **Lola González-García**[1,2,*]

[1] INM-Leibniz Institute for New Materials, Campus D2 2, 66123 Saarbrücken, Germany
[2] Saarland University, Department of Materials Science and Engineering,Campus D2 2, 66123 Saarbrücken, Germany
[*] Author to whom any correspondence should be addressed.

**E-mail:** lola.gonzalez-garcia@leibniz-inm.de

**Keywords:** electrofluids, emulsions, soft conductors, percolation, volume exclusion, strain thickening, mechanoelectrical properties

Supplementary material for this article is available online

## Abstract

A classical approach to reduce the percolation threshold in conductive polymer composites is the so-called volume exclusion. While this method proved to lower the filler concentration required to achieve electrical conductivity in solid composites, it remains unexplored for liquid conductive composites such as electrofluids (EFs). We propose the combination of emulsions and conductive particles to create EFs with reduced filler content. Conductive emulsions were prepared based on two immiscible liquids, glycerol and polydimethylsiloxane (PDMS), and carbon black (CB) as the conductive filler. The structural characterization of stable emulsions revealed a selective distribution of CB in the PDMS phase (continuous phase), around glycerol droplets (dispersed phase). This configuration led to a decrease in percolation threshold proving the viability of volume exclusion as strategy in EFs. The combination of the CB network and the glycerol droplets resulted in unpredictable mechanoelectrical properties such as a reduced stiffness scaling compared to CB-EFs in the pure solvents and the reduction of a strain thickening behavior with increased filler concentration. We evaluated the role of the CB in the emulsion formation and its impact on the droplet size and size distribution and concluded that this effect must be synergetic with the creation of a stress-carrying filler network that absorbs the elastic energy from the droplet deformation at large strains.

## 1. Introduction

Soft electronic components are of great interest for applications demanding stretchable sensors [1] or stable conductors [2], like wearables [3] or implants [4]. Conductive polymer composites are a common type of material to create electrical conductors with relatively low Young's modulus [5]. They consist of conductive filler particles dispersed in a non-conductive polymeric matrix, often elastomers. The high variety of conductive fillers and matrices confers on them a high versatility and a broad degree of tunability in their properties. For example, fillers can be found with different shapes and of different nature such as silver [6], copper [7], or gold [8] spherical particles; silver wires [6] or flakes [9]; carbon materials such as fractal carbon black (CB) [10], carbon nanotubes (CNTs) [11], and graphene flakes [12]; or 2D materials such as $MoS_2$ [13] or MXenes [14]. Depending on the filler and matrix combination, the minimum amount of filler required to create at least one conductive path throughout the composite volume, the so-called percolation threshold, might vary significantly [15]. Besides the economic considerations, reduced percolation thresholds are desired to minimize the reinforcement effects of increased filler loadings, which lead to stiffer composites [16] with reduced elongation at break [17]. Typical approaches for reduced percolation are the selection of high aspect ratio fillers like rods or wires [18–20] or inducing agglomeration by selecting low affinity matrices [21], restricting the possible combinations.

Another strategy to reduce the percolation threshold, independently of the filler shape and nature, is the so-called 'volume exclusion' using a third phase in the composite. The idea is to restrict the available volume for the filler, forcing the conductive network formation at lower concentrations. Three main approaches can be distinguished in conductive composites. First, double percolation systems rely on the preferential dispersion of the conductive filler in one polymer of an immiscible polymer blend. As both polymers form a percolative system, like found in heterojunctions, if the filler in turn forms a percolative network in its preferential phase, the overall composite turns conductive. Sumita *et al* employed such strategy by blending polypropylene (PP) with polymethylmethacrylate (PMMA) and adding CB as the conductive filler, which preferentially distributed in the PMMA phase [22]. Similarly, Li *et al*, prepared solid composites based on an immiscible blend of PP and epoxy with CB as the conductive filler. They found a percolation threshold of 7.4 wt.% in a 50:50 weight ratio of PP and epoxy. This was approximately half compared to the percolation threshold using only epoxy as the matrix (14.5 wt.% CB) [23]. Recently, Topcu *et al* reported a reduction of the percolation threshold of ca. 50% (from 0.46 vol.% to 0.19 vol.%) of multi-walled CNTs (MWCNTs) using a double percolation strategy with a mixture of polystyrene (PS) and ethylhexyl acrylate compared to the use of pure homopolymer of PS as a matrix [24]. Second, some types of segregated composites also make use of immiscible polymers but, in this approach, the filler locates at the polymer-polymer interface, which reduces further the volume available for it [25]. Chen *et al* studied the electrical conductivity of CNTs in a blend of polycarbonate (PC) and acrylonitrile-butadiene-styrene [26]. The selective localization of CNTs at the interface between these polymers led to a reduced percolation threshold of 0.05 wt.% for the segregated composite compared to the 0.24 wt.% CNT in pure PC [26]. Lastly, a relatively simpler approach uses a filling third phase, for example, non-conductive fillers, that are distributed in the composite matrix taking away available volume of the continuous phase for the conductive filler. Bao *et al* used solid particles of calcium carbonate ($CaCO_3$) as the third phase in a composite containing MWCNTs and PP [27]. They found that by adding 30 wt.% of $CaCO_3$ the electrical percolation threshold was lowered from 0.90 to 0.63 vol.% MWCNTs, attributed to the volume exclusion effect, that increased the effective MWCNT concentration in the polymer phase [27]. To alleviate the impact that such solid fillers might have on the macroscopic stiffness of the final composite, softer materials can be used [28].

All the above-mentioned approaches have been successfully applied in solid conductive composites to reduce the electrical percolation threshold. A new type of truly soft conductor are electrofluids (EFs), liquid composites containing conductive filler particles in a liquid matrix [29]. To the best of our knowledge, none of the volume exclusion approaches has been investigated in EFs so far. Due to the liquid nature of EFs, we propose the use of emulsions filled with conductive particles as a volume exclusion approach. An emulsion consists of two immiscible liquids, where the dispersed phase forms droplets to minimize the contact area with the so-called continuous phase [30]. By introducing the conductive filler in the continuous phase, the dispersed phase would act as volume exclusion component, leading to a reduced percolation threshold. The addition of particles to an emulsion has an impact on its stability. Koos reported a ternary phase diagram of a solid–liquid–liquid emulsion, indicating stable emulsions depending on the volume fractions of the constituents [31]. It was shown that an increase of the volume fraction of the filler's preferential phase transforms the emulsion from a pendular state to a capillary state [31]. In the work of Kandy *et al*, the effect of MWCNTs on the rheological properties of highly concentrated emulsions was studied [32]. They formed an emulsion based on an aqueous dispersed phase (water with ammonium salts) and a continuous oil phase (based on canola and paraffinic oil). Cryogenic scanning electron microscopy images revealed the selective assembly and formation of a 3D network of MWCNTs in the continuous oil phase of the emulsion. The presence of the filler impacted the droplet size and size distribution during the manufacturing process, leading to an increased shear viscosity and increased stiffness [32]. Although their rheological properties have been investigated, the conductive properties of such particle filled emulsions remain unexplored. Especially, the interplay between mechanical and electrical networks, which is determinant for their mechanoelectrical properties.

In this work, we report conductive emulsions as a volume exclusion strategy to lower the electrical percolation threshold in EFs. We investigated the stability of emulsions composed of polydimethylsiloxane (PDMS) and glycerol at different ratios and successfully created stable conductive emulsions, also when adding increasing amounts of CB. Electrical characterization revealed a reduction in the percolation threshold, consistent with the preferential dispersion of CB within the non-polar PDMS phase. This model was supported by optical microscopy images of CB-containing emulsions. Rheological characterization coupled with *in-situ* electrical measurements of the emulsions was performed to determine their mechanoelectrical properties and understand the interplay between the mechanical and the electrical networks. We observed that increasing CB concentration led to (a) increased stiffness of the emulsions and

(b) the suppression of the strain thickening at large amplitudes observed in pure emulsions. Two hypotheses are discussed to explain these effects: droplet size reduction and CB-network interaction with the droplets. Further analysis revealed that, although CB influences droplet size and size distribution, the dominant contribution to the mechanoelectrical response arises from the percolating network formed above its percolation threshold in the continuous phase, which affects the coherent mechanical properties of the droplets.

## 2. Results and discussion

The emulsions were prepared mixing glycerol (polar) and polydimethylsiloxane (PDMS, non-polar), as immiscible liquids [33]. After mixing, the emulsions span homogeneously the whole sample volume (see figure S1(A) of the supporting information). To determine the optimum ratio of the liquids and maximize the emulsion stability, different mixtures were prepared at increasing PDMS concentration (see Methods section for details), and their stability was assessed by means of analytical centrifugation (AC). Figure 1(A) shows the cuvettes with PDMS/glycerol emulsions after the AC protocol and figure 1(C) shows the percentage of the emulsion phase that remained stable after the test (open circles).

During centrifugation, the excess of the pure liquids separated due to their different densities (0.97 and 1.26 g $cm^{-3}$ for PDMS and glycerol, respectively) revealing the stable emulsion fraction, clearly distinguished due to its turbidity (see figure 1(A)). The layer at the top of the cuvette corresponds to PDMS and the one at the bottom to glycerol. Optical microscopy images revealed that the emulsion is formed by glycerol droplets that are dispersed within the PDMS phase (see figure S1(B) of the supporting information). Since the emulsion contains both liquids, the effective density lays between the one of PDMS and glycerol, therefore, it laid in the middle, separating the pure solvent phases. At increasing PDMS concentration, the emulsion phase shifted downwards, due to the increasing amount of low-density phase, until a critical concentration was reached, at which the emulsion was sufficiently stable to sustain the AC test. These stable emulsions were observed for a certain ratio range, while higher concentrations of PDMS led to phase separation after the AC test. To determine the critical composition range for stable emulsions, we quantified the percentage of the emulsion phase present in the cuvettes after the AC test at increasing PDMS concentration (see open circles in figure 1(C)). Note that the AC test was performed at a relative centrifugation force (rcf) of 2350 *g* during 20 h, which is equivalent to a long-term stability test of ca. 5 years in storage conditions (1 *g*). The transmission threshold between the phases in the AC test was set to 20% (see Methods section and figure S2 of the supporting information for details). As expected from the photographs, the percentage of emulsion phase increased gradually with rising PDMS concentration up to a 50:50 ratio, beyond which a pronounced increase in the phase growth was observed. Stable emulsions (over 95% of emulsion phase) were found in the range of 56 vol.% to 60 vol.% of PDMS in glycerol, with the maximum (∼97% of emulsion phase present) found for 58 vol.% of PDMS. We calculated the instability index for this emulsion and found a value of 0.033, indicating marginal changes in its stability during the test. Moreover, the sedimentation velocity was also estimated based on the transmission changes during the AC test, resulting in 2.1 $\mu$m $s^{-1}$, which corresponds to $\sim 0.9 \cdot 10^{-3}$ $\mu$m $s^{-1}$ at 1 *g*. Further addition of PDMS reduced the emulsion proportion and induced the separation of the excess of PDMS, visible at the top of the cuvette. A similar trend was observed in oil-in-water emulsions composed of corn oil and oleic acid (oil phase) and sodium carboxymethylcellulose, triethanolamine, and water (aqueous phase). The authors reported that the stability of the emulsion increased with increasing dispersed phase (oil phase) content [34].

Carbon black (CB) was selected as the conductive filler to create a percolating network and confer the material of electrical conductivity. Previous reports showed that the addition of solid fillers to an emulsion may change its stability depending on the type of filler [35, 36]. To exclude that, the same AC test was performed with the PDMS/glycerol mixtures adding a small amount of CB. After mixing, the CB was evenly distributed over the entire volume (see figure S1(C) of the supporting information). Photographs of the cuvettes after the AC protocol are shown in figure 1(B). With the addition of CB, below the critical concentration (low PDMS ratios) only two different phases can be distinguished: a black phase on top and a clear phase at the bottom. Due to the hydrophobic nature of its surface, CB has a higher affinity towards the PDMS phase [29]; CB was, therefore, present in both, the pure PDMS phase (top) and the emulsion phase (within the PDMS), making undistinguishable among them both while the glycerol remained clear. When reaching the critical concentration for stable emulsions, a homogeneous black phase was observed. The AC analysis (filled circles in figure 1(C)) revealed a similar trend compared to the samples without CB (open circles in figure 1(C)). However, one must notice that, with CB, the pure PDMS phase and the emulsion phase are indistinguishable, provoking an overestimation of the second one in the graph, particularly at high PDMS contents. At low PDMS ratios, a

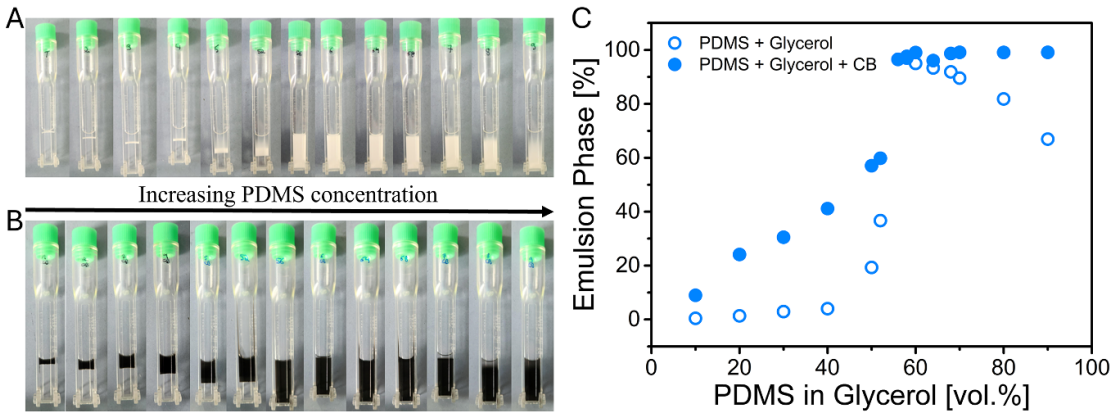


**Figure 1.** Polyamide AC cuvettes filled with PDMS/glycerol emulsions with different concentrations of PDMS in glycerol (A) without and (B) with CB after analytical centrifugation. (C) Percentage of the emulsion phase of the total volume, that remained stable after the AC test, for different concentrations of PDMS in glycerol. Open symbols refer to pure emulsions and closed symbols refer to CB-containing emulsions.

more gradual increase was observed also due to this overestimation, while at high PDMS volume ratios, the graph reached a plateau. Mazurek *et al* found a similar behavior when they studied PDMS/glycerol mixtures [33]. They investigated the viscosity of the emulsions of different ratios and found an increase with increasing glycerol concentration. The maximum in viscosity was found at approximately 48 vol.% of glycerol in the mixture (52 vol.% of PDMS), close to our stable emulsion composition: 58 vol.% PDMS. One must notice that the small discrepancy can be caused due to the emulsion preparation procedure or the stability evaluation method, they followed the evolution of the viscosity while we focus here on their stability by AC. The instability index and the sedimentation velocity for this combination were also calculated from the AC test, leading to 0.048 and $1.2{\cdot}10^{-3}$ $\mu$m $s^{-1}$ at 1 *g*, respectively, close to the values obtained for the corresponding pure emulsion. From this point onward, all further experiments were conducted using the emulsion with 58 vol.% PDMS in glycerol.

The addition of a conductive filler to a liquid matrix only leads to a conductive network if the concentration of filler is high enough to ensure the creation of a continuous path that spans the entire volume. This minimum concentration is defined as the percolation threshold ($\phi_c$) and is related to the electrical conductivity ($\sigma$) by the formula: $\sigma = A(\phi - \phi_c)^t$, where $A$ is a constant, $\phi$ is the filler fraction, and $t$ is a critical exponent [15]. To determine the percolation threshold of the CB in the emulsion, we measured the electrical conductivity of emulsions at increasing CB concentration using a 4-point-probe set up (see Methods section for details). Figure 2(A) shows the percolation curve of CB in the emulsion system (blue circles) compared to those of CB-EFs in pure PDMS (grey circles) and pure glycerol (black circles) extracted from [29].

The percolation threshold of CB in the emulsion was found at 4.78 wt.% CB, which laid between that reported for the two pure solvents 0.65 wt.% CB and 8.33 wt.% CB for glycerol and PDMS, respectively [29]. If we assume that the CB is solely dispersed in the PDMS phase, the normalization of CB content in the emulsion to the amount of PDMS must fit to this second value. The normalized percolation curve is displayed as cyan, open square symbols in figure 2(A), and the fitting delivered a critical concentration for percolation of 8.88 wt.% CB, which deviates less than 6% from the previously reported value for CB in pure PDMS [29].

To confirm that CB distributes preferentially in the PDMS phase around the glycerol droplets, we recorded optical microscopy images of a 3 wt.% CB-emulsion (see figures 2(B) and S3 of the supporting information). Clear droplets were distinguishable in the micrographs while the CB was surrounding them, dispersed in the continuous phase. Imagine CB in pure PDMS at a concentration of 5 wt.% (below the percolation threshold), the fillers are then well-dispersed, and the connectivity is not sufficient to create a percolating path (see figure 3(A)). Imagine now the same amount of CB in the emulsion; glycerol droplets take out part of the volume, that is no longer available for CB particles. They are, therefore, forced into a restricted volume around the droplets. As a result, the agglomerates become larger, inducing the formation of a percolated pathway at lower concentrations than in the pure PDMS matrix (see figure 3(B)). This explains the reduced percolation threshold by volume exclusion for EFs.

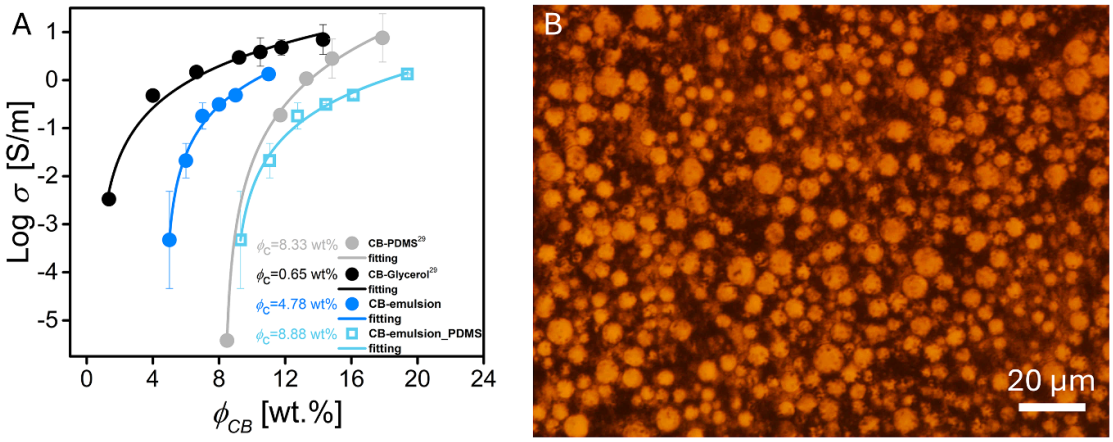


**Figure 2.** (A) Electrical percolation curves of CB in different liquids. Grey, closed circles: PDMS [29], black, closed circles: glycerol [29], blue, closed circles: PDMS/glycerol emulsion, cyan, open squares: emulsion PDMS/glycerol normalized to the weight of PDMS in the emulsion. Solid lines are fit functions according to classical percolation theory $\sigma = A(\phi - \phi_c)^t$ [15]. The concentration of the percolation threshold derived from the fit function corresponding to each system are noted in the graph. (B) Optical microscopy image of a PDMS/glycerol emulsion filled with 3 wt.% CB with a 50x magnification.

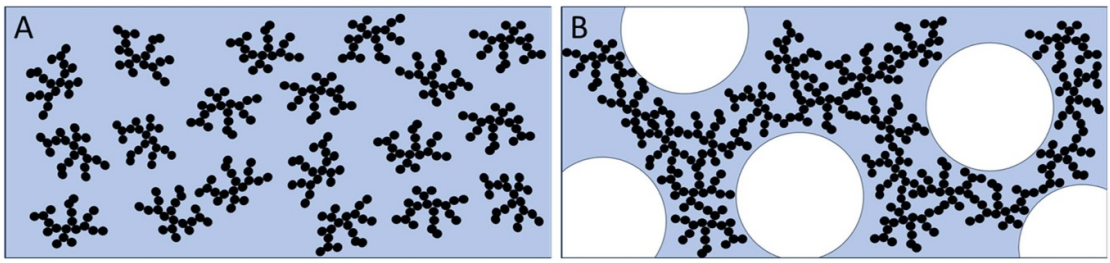


**Figure 3.** (A) CB dispersed in pure PDMS at a concentration below the percolation threshold (<8.33 wt.%). (B) Volume exclusion concept for CB-emulsions. CB dispersed in PDMS at the same concentration with glycerol droplets taking out 39.7% of the space (under the assumption of additive volumes).

The addition of conductive solid particles to simple liquid matrices in concentrations above the percolation threshold renders the suspension electrically conductive but increases the stiffness and the viscosity concomitantly. This behavior was observed, for example, in EFs based on CB suspensions in pure glycerol and PDMS [29]. The case of emulsions as matrices is, however, more complex: the presence of a high concentration of droplets typically leads to an enormous increase of the viscosity compared to the constituent liquids. This increase is due to the elasticity of the droplets caused by the surface energy and depends on the droplet concentration and size [37]. When adding particles to this system, multiple interactions between the droplets, the filler, and the continuous phase influence the final mechanoelectrical properties. Therefore, the trade-off between conductivity and elasticity for conductive emulsions might differ compared to simple conductive suspensions. To evaluate the flow behavior and viscosity of emulsions at different filler concentrations, rotational rheology was performed. The electrical resistance was monitored *in-situ* giving access to the electrical network during the mechanical deformation. Figure 4(A) shows the flow curves (and electrical resistance for conductive systems) of the pure solvents (PDMS and glycerol), the pure emulsion (58 vol.% PDMS in glycerol), and CB-emulsions at different concentrations.

Compared to the pure solvents, all emulsions showed increased viscosity at low shear rates. Only the presence of glycerol droplets (without CB) increased 35 times the viscosity compared to pure PDMS. We observed that the addition of CB filler increased further the low shear viscosity even at concentrations below the electrical percolation. This phenomena is attributed to the internal resistance against deformation that builds up by fillers [38]. Additionally, all emulsions (with and without CB) presented a shear thinning flow behavior (viscosity decreases with increasing shear rate) in contrast to the pure solvents that presented a Newtonian flow behavior (independent viscosity value). At higher shear rates, the droplets deform and align in the flow direction reducing the resistance to flow (viscosity) and promoting a shear thinning behavior. Similar observations are reported in literature for oil-in-water and water-in-oil emulsions [39, 40]. The addition of CB also increased the degree of shear thinning, defined

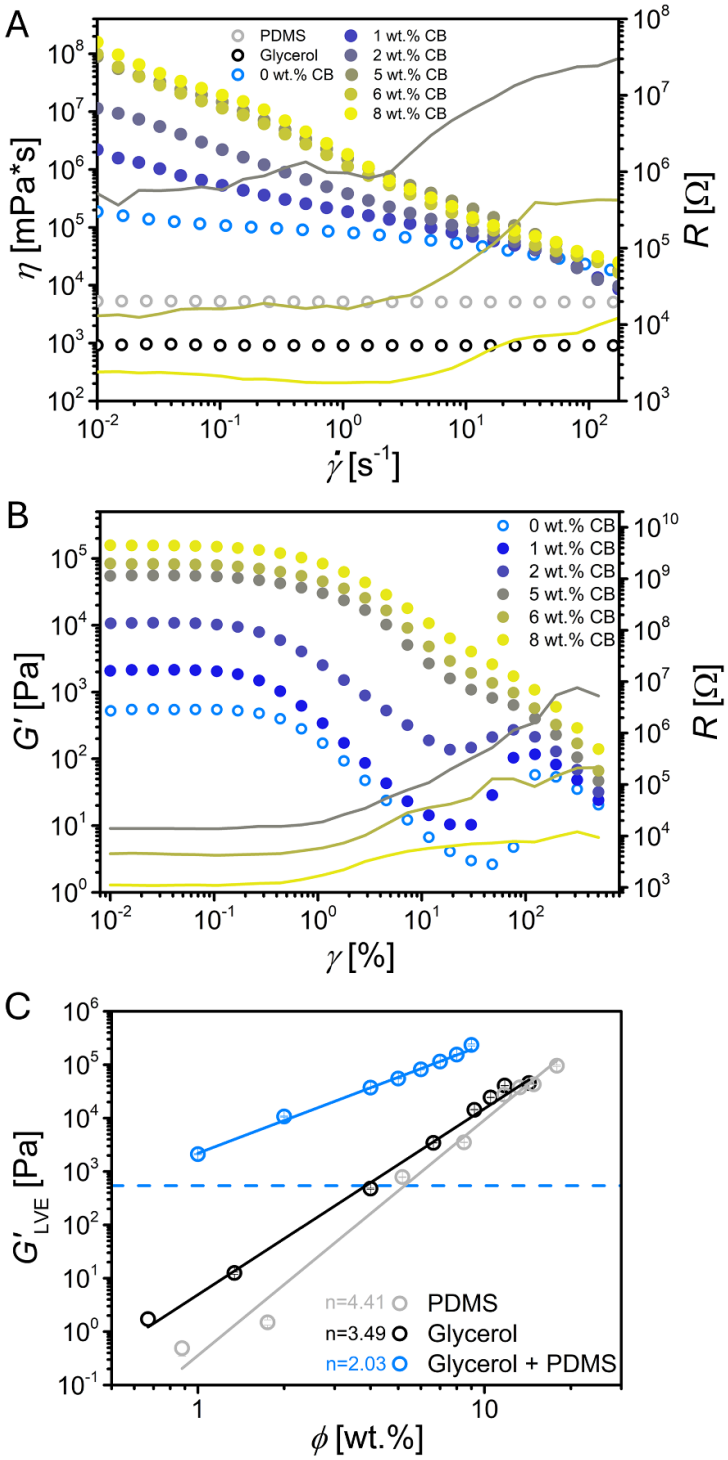


**Figure 4.** (A) Flow curves of the pure solvents (grey, open circles: PDMS, black, open circles: glycerol), PDMS/glycerol emulsion (cyan, open circles), and CB-emulsions at increasing CB concentration (closed circles from dark blue to bright yellow at increasing CB concentration). Solid lines with the same color code represent the electrical resistance values measured during the flow curve for electrically conductive CB-emulsions (weight percentages below 4 wt.% were not electrically conductive, thus are not shown). (B) Amplitude sweeps of PDMS/glycerol emulsions and CB-emulsions at increasing CB concentration. The symbol and color code are the same as in the previous panel. Solid lines represent the resistance measured during the test at each strain value. (C) Storage modulus ($G'$) at the LVE-region vs. CB weight percentage for grey: CB in PDMS [29], black: CB in glycerol [29], and cyan: CB in PDMS/glycerol emulsion. Dashed line denotes the $G'$ value of the unfilled emulsion. Solid lines are fit functions based on power law scaling $G' \propto \phi^n$.

by a steeper slope in the flow curve [41]. At low shear rates, the viscosity increased with the CB concentration in the emulsions since the particles oppose to the flow. When filler particles are aligned under shear deformation (higher shear rates), the denser filler network loses more interparticle connections,

which results in a stronger shear thinning. At very high shear rates, the influence of the CB in the viscosity is basically negligible and all the emulsions reach approximately the same viscosity value.

The electrical resistance, which only depends on the CB network, remained constant at low shear rates (small changes are attributed to the scattering of the measurements). Under this deformation, the breaking rate of the transient contacts between the particles is then equivalent to the forming connection rate, retaining the electrical properties. When the critical shear rate $\dot{\gamma}_{crit} \approx 2\ s^{-1}$ was reached, the resistance started to increase due to the increase of the breaking connection rate that was no longer compensated with the formation of new connections. This critical shear rate was independent of the CB concentration in this study. A similar behavior was recently reported for EFs based on MWCNTs in pure glycerol [42]. Under shear flow, EFs kept their electrical conductivity constant until a critical shear rate, which was also independent of the MWCNT concentration. In contrast to our work, the MWCNT-based EFs lost their electrical conductivity completely at shear rates above 50 $s^{-1}$ [42], while CB-emulsion EFs showed different increments of the resistance but preserved electrical conductivity in all studied cases. The different behaviors found in these two types of EFs can be attributed to (a) the constrained volume in the CB-emulsions that restricts the mobility of the filler under shear flow and increases the probability of filler-filler contacts and (b) the poor alignment of CB due to their fractal morphology. MWCNTs exhibit a high aspect ratio and remain unconfined within the EFs, which promotes their alignment along the shear direction while disrupting connectivity in the perpendicular direction to the flow field (direction of electrical measurement).

To further understand the interplay between the glycerol droplets and the CB network in conferring the mechanical properties of the emulsions, we analyzed their elastic and viscous responses by means of oscillatory amplitude sweeps at 10 rad $s^{-1}$ (see details in the section Methods). Additionally, we measured the electrical resistance, to track the impact of deformation on the conductive CB network. The storage modulus ($G'$) in relation to the applied shear strain is depicted in figure 4(B) while the corresponding loss modulus ($G''$) is shown in figure S4 of the supporting information. Three different regimes can be distinguished in the mechanical response of all emulsions. The small amplitude oscillatory shear (SAOS) assesses the elastic behavior of the material. This region of small deformations is defined by the so-called linear viscoelastic (LVE) region, where $G'$ is independent of the applied shear strain. The $G'$ value in this region is a measure of the stiffness of the material [43]. With increasing CB concentration, the $G'$ value increased from an initial value of 550 Pa (for the pure emulsion) to almost 158 MPa (at 8 wt.% CB), which means an increase of three orders of magnitude in stiffness. Analogous to the invariant $G'$, at this low strain deformation, the electrical resistance also showed a plateau value. The initial resistance in this case decreased the higher the CB concentration was, as expected from the percolation curve. At larger deformations, when the $G'$ deviates more than 3% from the plateau value (typically by a decrease), the medium amplitude oscillatory shear (MAOS) region, or yield zone, starts [41]. This initial point, known as yield point ($\tau_{yield}$), quantifies the maximum stress that the material stores as elastic energy. From this point on, the mechanical network undergoes plastic deformations. This region extends up to the flow point—the stress, at which the material transitions from a solid-like to a liquid-like behavior ($\tau_{flow}$)—and it is visible in the amplitude sweep as the crossover between $G'$ and $G''$. Within the MAOS region, an increase in the electrical resistance of the conductive samples was observed (see figure S4 of the supporting information). Similarly to the yield stress, we define an electrical yield stress ($\tau_{el.\ yield}$) as the stress needed to increase the initial resistance by 10%. The comparison between these three parameters (yield point, flow point, and electrical yield) as functions of the CB content is shown in figure S5 in the supporting information. All three showed a power law scaling with CB concentration. A similar scaling law of the yield stress of different particle suspensions was previously reported [44, 45] and attributed to a transition from disordered particle interactions to ordered structures [45]. No previous reports were found for the flow point and the electrical yield stress. The electrical yield stress appeared at approximately 1/3 of the flow stress for all studied samples, indicating that large distortions in the mechanical CB network must occur prior, affecting the electrical network.

Strains beyond the flow point are considered to be in the large amplitude oscillatory shear (LAOS) region. Here, the network strength is not sufficient to sustain the stress, and the material behaves as a liquid. In this region, a continuous decay of the moduli is expected as often observed in complex fluids, *i.e.*, polymer melts, particle suspensions, or emulsions [46]. We, however, observed an increase in $G'$ and $G''$ for the pure emulsion and those with CB content below the electrical percolation threshold (1 and 2 wt.%). This phenomenon, called strain thickening, has been reported in some highly concentrated particle suspensions [47–49]. Although still under discussion, the last studies point particle jamming due to frictional contacts that generate a frictional network as the cause of the increased elastic modulus [50]. In emulsions, such behavior has so far only been reported in particle-stabilized systems [51, 52];

however, the underlying mechanism remains unclear. We observed that, with increasing CB concentration, the intensity of the strain thickening decreased, turning to a small shoulder at 5 wt.% CB, which coincided with the transition to the electrical network formation (percolation threshold of 4.78 wt.% CB). At this point, two hypotheses could explain how the presence of CB inhibits the strain thickening effect: (a) the CB filler induces a change in mean droplet size during the mixing process, influencing the strain thickening effect and (b) the CB filler network hinders the droplet-droplet contact and absorbs the elastic energy originated from droplet deformation. These two hypotheses are revised below in this text.

Figure 4(C) shows the relation of the storage modulus at the LVE-region, as a measure of the stiffness of a material, with the CB concentration for the selected emulsion and the CB-EFs using pure solvents extracted from [29]. The value of *G*' for the unfilled emulsion is shown by a light blue dashed line. This value (544 Pa) is similar to the one found for 4 wt.% filler loading in a glycerol CB-EF (479 Pa). The CB-emulsions exhibit *G*' values above the CB-EFs in both glycerol and PDMS, due to the high elastic deformation that the glycerol droplets uptake. The *G*' of all EFs scaled with a power law of the type $G' \propto \phi^n$, giving different scaling exponents that depend on the filler network and the filler-matrix interactions. Previous reports show that in combinations where the filler-solvent interactions dominate (high affinity between them as in the case of CB-PDMS), the resulting exponent is larger due to the additional reinforcement contribution compared to those, in which the stiffness is solely a result of the filler-filler interactions (low affinity as in the case of CB-glycerol) [29]. In the emulsion, the continuous phase is PDMS, where the CB is localized. A similar scaling exponent than that for CB-PDMS ($n = 4.41$) with an offset from the initial *G*' of the pure emulsion was, therefore, expected. The obtained exponent from the fitting is, on the contrary, lower than that for CB-Glycerol ($n = 2.03$ and $n = 3.49$, respectively). This result is compatible with both of our previous hypotheses. On one hand, if the CB influences the glycerol droplet size during the mixing, smaller droplets may interfere with the CB-CB interactions, reducing their contribution to stiffness. On the other hand, the elastic scaling exponent would also be reduced if the CB network absorbs the elastic energy from the droplets' deformation.

To test the first hypothesis, we investigated the influence of the CB on the glycerol droplet size using optical microscopy image analysis of emulsions at different filler concentrations. Exemplary micrographs are shown in figures 5(A)–(C) for CB-emulsions with filler loadings of 3, 5, and 7 wt.% CB. Additional micrographs used for image analysis are displayed in figure S6 of the supporting information.

To quantify the droplet size, the images were processed using a commercial analysis software (see Methods section and figure S7 of the supporting information for details) and the mean equivalent diameter was calculated. We observed a decrease in the average droplet size with increasing CB concentration, up to a 32.2% for 7 wt.% CB (figure 5(D)). This effect is in good agreement with previous reports, in which a decrease of droplet size in a water-in-oil emulsion was observed as a consequence of the presence of a stiff filler, such as CNTs, that disrupts the droplets during the mixing process [32, 54]. To analyze the impact of this reduction in size on the mechanical properties, Mudeme *et al* used a modified power law of the form $G' = K \cdot d^{-m}$ (where $K$ is a constant, $d$ is the droplet diameter, and $m$ a fitting exponent)[53] based on the Princen–Kiss model ($G' \propto d^{-1}$) [55] and the Malkin model ($G' \propto d^{-2}$) [56]. These models, developed in particular for highly concentrated emulsions (HCEs), attribute the increase of elastic modulus with decreasing droplet size to the interfacial energy stored caused by a compression of droplets at emulsion concentrations above packing density [57]. The original models proposed universal exponents of 1 and 2; however, Mudeme *et al* reported exponents between 1.67 and 2.25 for different emulsions. Variations in the experimental exponent have been attributed to the concentration of the dispersed phase [56, 58], the droplet polydispersity [56], and the use of surfactants that change droplet interactions [59]. The emulsion in this work contains less dispersed phase fraction than required to be classified as HCE ($\phi = 0.42$ compared to $\phi = 0.64$ for random close packing). Nevertheless, we tested the unfilled 58 vol.% PDMS in glycerol emulsion with different droplet sizes, achieved by varying the rpm during the mixing process (see Methods section for details) for their elastic scaling to be compared with literature values. The scaling exponent of the elastic modulus with $d^{-1}$ was found to be $m = 1.09$ (see figure S8 of the supporting information). This value, very close to 1, suggested a good correlation with the theoretical Princen–Kiss model. We used the same equation to evaluate the scaling of *G*' of CB-containing emulsions since increasing filler content led to a reduction of the average droplet size. The fitting depicted in figure 5(E) shows an exponent of $m = 9.83$, far from any values reported of unfilled emulsions. The reduction of the droplet size by its own cannot explain the scaling variation of *G*' found in this study. Another factor to be considered is the impact that smaller droplets have on the strain thickening effect. As described above, we found a decrease of the strain thickening at increasing CB concentration in the emulsions. We performed amplitude sweeps of the unfilled emulsions with different droplet sizes (see figure S9(A) of the supporting information) and calculated the strain thickening ratio, *i.e.,* the ratio between the highest *G*' value in the thickening regime and the *G*' value before the increase

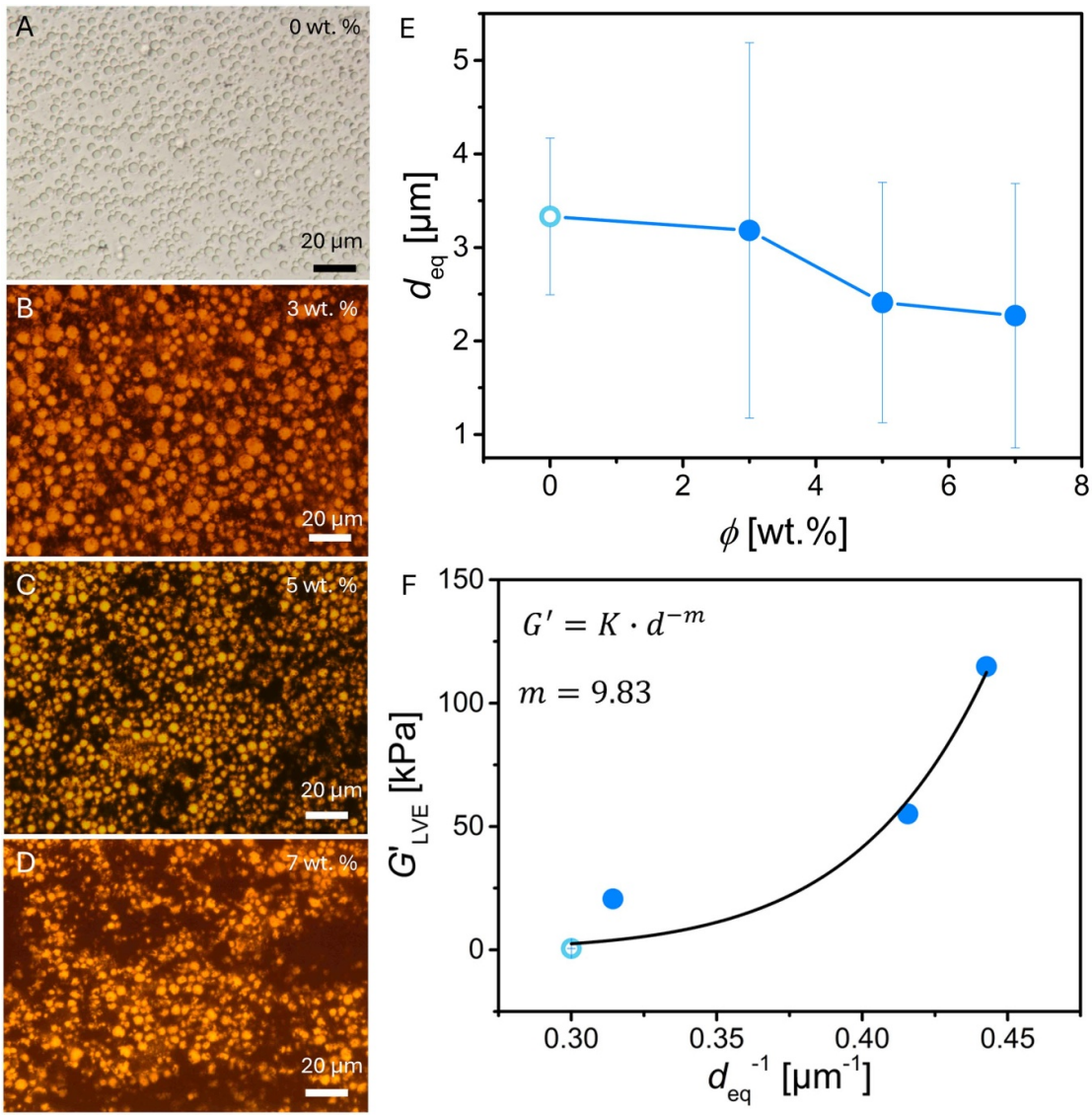


**Figure 5.** Optical microscopy images of PDMS/glycerol emulsions filled with (A) 0, (B) 3, (C) 5, and (D) 7 wt.% CB. (E) Mean equivalent diameter of glycerol droplets depending on the weight percentage of CB. Cyan, open circle indicates the pure emulsion values and blue, closed circles the values for the CB-emulsion; lines are a guide to the eye. (F) Plateau storage modulus of the pure emulsion (cyan, open circle) and CB-containing emulsions (blue, closed circles) depending on the inverse droplet diameter. The black line is a power law fit according to [53].

(see figure S9(B) of the supporting information). The reduction in droplet size caused an increase of the strain thickening effect in the pure emulsion. This is the opposite result of what we observed in the CB-containing emulsions. Therefore, the changes described in this study cannot be attributed to the reduced droplet size of the glycerol droplets by the presence of CB. We believe that both effects, reduced stiffness scaling and suppressed strain thickening, are related to the difference in elastic modulus between CB network and glycerol droplets. The presence of glycerol droplets causes a weaker scaling of stiffness of the CB network due to their lower elastic modulus. At high deformations (LAOS region), the CB network around the droplets acts as a stress-carrying network, transporting and distributing the elastic energy, which leads to the suppression of the strain thickening effect.

## 3. Conclusion

In this study, we presented stable, electrically conductive emulsions, based on selective distribution of CB filler in PDMS and glycerol mixtures. Analytical centrifugation revealed an optimum ratio of 58 vol.% PDMS in glycerol for emulsion stability. The addition of CB rendered the emulsion conductive at half of the concentration for the electrical percolation threshold of CB-PDMS EFs. This is consistent with

the proposed model, in which the CB particles (hydrophobic) tend to disperse better in PDMS (non-polar, continuous phase) than in glycerol (polar, dispersed phase). The glycerol droplets act, therefore, as volume exclusion component proving the feasibility of this strategy in liquid composites. The normalization of the CB concentration to the PDMS amount in the emulsion deviated less than 6% to that reported for CB-PDMS EFs. Unique mechanical properties of the CB-emulsions were found, such as a strain thickening behavior at low CB contents and a reduced scaling exponent of the storage modulus with increased filler concentration. The impact of the presence of CB in the emulsion preparation was evaluated by image analysis of optical micrographs. A reduction of glycerol droplet size was observed, laying the foundations of one of the hypotheses to explain the mechanical behavior of the CB-emulsions. Further analysis using pure emulsions with variable droplet size revealed this to not be the only effect governing the mechanical properties found in CB-emulsions. We believe that the presence of filler particles, particularly above the percolation threshold, creates a stress-carrying network around the glycerol droplets, that acts as a damping material and absorbs the elastic energy formed by droplet deformation. Concomitantly, the contribution of CB to the scaling of storage modulus of the emulsions at increasing filler content is significantly reduced due to the presence of glycerol droplets compared to CB-EFs based on pure solvents. We envision the rational design of emulsion-based EFs through the selective combination of solvents and fillers, enabling a broad range of tunable mechanoelectrical properties. The predictability of these properties, however, remains limited due to the current lack of comprehensive research.

Carbon-based EFs have demonstrated utility as strain sensors [60], stable conductors [29], and conductive greases [42]. The emulsion-based EFs introduced here add a further dimension of tunability to their mechanoelectrical properties, thereby broadening their applicability range. Moreover, these emulsions deliver electrical performance comparable to single-solvent EFs while exhibiting substantially higher viscosities. Elevated viscosities mitigate sedimentation, enabling the use of dense metal fillers—such as silver particles or flakes—to yield EFs with markedly higher electrical conductivity, approaching that of liquid metals. Collectively, these advances position emulsion-based EFs as a versatile platform for soft, reconfigurable, and high-conductivity devices.

## 4. Methods

### 4.1. Sample preparation

Sylgard 184 (Dow Corning, USA) and glycerol ReagentPlus ⩾99% (SigmaAldrich, Germany) were used as immiscible phases to prepare the emulsions and the carbon black (CB) used as filler was acetylene black, 100% compressed (Alfa Aesar, Germany). All chemicals were used as received. To create the emulsions, Sylgard 184 and glycerol were weighed into a cup and mixed with a DAC150.3 SP speed-mixer (Hauschild, Germany) at 3500 rpm for 5 min. For the CB-emulsions, CB was weighed and subsequently, the two liquids added to the same cup. The mixing protocol was the same as for pure emulsions. Inspired by previous reports [33, 61, 62], pure emulsions with varying droplet sizes were prepared using the same PDMS/glycerol ratio (58:42) but using different rpm values (1000, 1500, and 2000 rpm) for 5 min.

### 4.2. Analytical centrifugation

The prepared emulsions were filled with a syringe into 2 mm rectangular polyamide cuvettes. The cuvettes were put into a LUMiSizer 6510 (LUM, Germany) and centrifuged at 2350 rcf for 20 h. Transmission profiles were recorded during this time. A transmission threshold of 20% was chosen to distinguish the turbid emulsion phase from the transparent PDMS and glycerol phase (see figure S2 of the supporting information). The percentage of emulsion in the cuvette was calculated by measuring the length of the emulsion phase in the cuvette and dividing by the total length of the filled cuvette.

### 4.3. Optical microscopy

Emulsions were placed on a glass slide (Carl Roth, Germany) and covered with a cover glass (VWR, USA). The cover glass was firmly pressed and slid onto the sample to achieve a thin layer by shear. A Nikon Eclipse LV100ND (Nikon, Japan) microscope was used to record the images. The images were taken in transmission mode.

### 4.4. Electrical conductivity measurements

The CB-emulsions were transferred into a Teflon® mold with the dimensions 1.5 × 1.5 × 0.5 $cm^3$. A 4-point probe setup connected to a Keithley 2350 sourcemeter (Tectronix, USA) was used to apply a current sweep and measure the resulting voltage. The fit of the $I$–$V$-curve was a linear regression, and the

resistance was calculated from the slope value. The conductivity was derived by applying the following equation $\sigma = 1/(2{\cdot}\pi{\cdot}s{\cdot}R)$, where $\sigma$ is the conductivity, $s$ is the distance between the electrodes (1 mm), and $R$ is the measured resistance.

### 4.5. Rheoelectrical characterization

Rheology of the unfilled emulsions was performed using a MCR302e rheometer (Anton-Paar, Austria), with a concentric cylinder geometry (CC17) at a temperature of 25 °C. The bob was immersed slowly into the cup. A preshear of 175 $s^{-1}$ for 30 s was applied followed by 15 min resting prior to the flow curves and the amplitude sweeps. Former ones were conducted at shear rates between 0.01 and 150 $s^{-1}$ and the latter ones at strain values from 0.01 to 500%.

The characterization of the CB-emulsions was done in a MCR702e MultiDrive rheometer (Anton-Paar, Austria), in a 25 mm plate-plate configuration at 25 °C. The geometry was lowered slowly onto the sample and was let rest for 20 min to release initial stresses. Flow curves and amplitude sweeps were recorded at the same conditions as described above for the unfilled emulsions. For the electrical characterization, the upper and the lower geometries were connected to a Keysight E4980A LCR-meter (Keysight, USA). The LCR-meter was controlled with a python script to measure the resistance at each rheological measurement point.

The plateau value of the storage modulus ($G'$) was calculated by taking the average $G'$ of all points within the LVE region. The yield point was defined as the point where $G'$ deviates 3% compared to the plateau values.

### 4.6. Image analysis

Images for unfilled emulsions were segmented using the ImageJ Plugin WEKA [63]. Due to the poor contrast between glycerol droplets and PDMS, we marked several areas by hand and ran the WEKA algorithm to match the desired segmentation into two phases; PDMS and CB and glycerol droplets. For all other images, the commercial image analysis software Avizo (Avizo for EM-Systems, Thermo Fisher Scientific, USA) was used to determine droplet sizes. The optical micrographs were imported as 8-bit RGBA '.jpg' images of a size 2560 × 1920 pixels. Their physical pixel size was 68 nm due to the magnification in the optical microscope of 50x. The images were converted to 8-bit grayscale images (see figure S7(A) of the supporting information). Non-local means filtering (10 px search window, 3 px local neighborhood) was employed to denoise the images prior to segmentation (see figure S7(B) of the supporting information). Manual grayscale histogram thresholding was used to segment the droplet phase of the images. The threshold was set approximately at the minimum between the two peaks (see insert in figure S7(B) of the supporting information). The result was a binary image consisting of pixels corresponding to the droplet phase and the 'background' phase, *i.e.*, PDMS + CB (see figure S7(C) of the supporting information). Additional filtering artifacts were removed using the functions 'Despeckle' (7 px Kernel Size in $x/y$), which removes single pixels that did not correspond to droplets and 'Remove Small holes', which closes gaps in segmented droplets (see figure S7(D) of the supporting information). The final binary image was converted to a label image (see figure S7(E) of the supporting information), where groups of connected pixels were identified as single droplets. In the label image, different droplets have different 'labels' (numbers) assigned to them. Avizo provides functions to convert binary images to label ones: first, neighboring but apparently connected droplets need to be separated using the 'Separate Objects' function, which employs a watershed-segmentation on a distance-transformed binary input image to split the droplets. Afterwards, the split objects are labeled (function 'Labeling' with a 26-neighborhood) to obtain the label image. Droplets on the image border were removed from the label image using the 'Border Kill' function (see figure S7(F) of the supporting information). Finally, every unique label, *i.e.*, droplet in the border-killed label image was analyzed using the 'Label Analysis' module. Label areas $A_i$ for every label $i$ were computed by counting the number of pixels of the label and multiplying it by the physical size. The area-equivalent diameter $d_{eq,i}$ was computed as

$$d_{eq,i} = 2\sqrt{\frac{A_i}{\pi}}. \tag{1}$$

Additionally, the circularity for every label $\psi_i$ was calculated as

$$\psi_i = \frac{4\pi A_i}{P_i^2} \tag{2}$$

where $P$ is the perimeter of the label. Perfect circular droplets have $\psi = 1$, less-circular ones have $\psi \in (0,1)$. To exclude droplets that appeared visibly damaged we filtered our label analysis by allowing only

labels with $\psi > 0.3$. Average area-equivalent diameters $\bar{d}_{eq}$ were obtained by

$$\bar{d}_{eq} = \frac{1}{N}\sum_{i}^{N} d_{eq,i}. \quad (3)$$

## Data Availability Statement

All data that support the findings of this study are included within the article (and any supplementary files).

Supplementary Information available at http://doi.org/10.1088/2515-7639/ae3e18/data1

## Acknowledgments

The authors acknowledge funding by the European Research Council (ERC) under the European Union's Horizon 2020 research and innovation program (Grant Agreement No. 949785 ELECTROFLUID). The authors thank Miguel Baños Maestro for his help acquiring optical microscopy images, Minh Quan Bui and Simon Blum for technical support, and Sergio Lago-Garrido, Niclas Hautz, and Gun Woo Park for fruitful discussions.

## Author contributions

Dominik S Schmidt 0009-0008-5388-861X
Conceptualization (lead), Data curation (lead), Formal analysis (lead), Investigation (equal), Methodology (equal), Validation (equal), Writing – original draft (lead), Writing – review & editing (equal)

Dominik Perius 0009-0009-7579-7425
Formal analysis (supporting), Investigation (supporting), Methodology (supporting), Software (lead), Writing – review & editing (equal)

Lola González-García 0000-0002-8474-6517
Conceptualization (equal), Investigation (equal), Project administration (lead), Resources (lead), Supervision (lead), Visualization (equal), Writing – review & editing (equal)

## References

[1] Chossat J-B, Park Y-L, Wood R J and Duchaine V 2013 A soft strain sensor based on ionic and metal liquids *IEEE Sens. J.* **13** 3405–14
[2] Markvicka E J, Bartlett M D, Huang X and Majidi C 2018 An autonomously electrically self-healing liquid metal–elastomer composite for robust soft-matter robotics and electronics *Nat. Mater.* **17** 618–24
[3] Lyu Q, Gong S, Yin J, Dyson J M and Cheng W 2021 Soft wearable healthcare materials and devices *Adv. Healthcare Mater.* **10** 2100577
[4] Xu L *et al* 2014 3D multifunctional integumentary membranes for spatiotemporal cardiac measurements and stimulation across the entire epicardium *Nat. Commun.* **5** 3329
[5] Liu H *et al* 2018 Electrically conductive polymer composites for smart flexible strain sensors: a critical review *J. Mater. Chem. C* **6** 12121–41
[6] Yu Y-H, Ma C-C M, Teng C-C, Huang Y-L, Lee S-H, Wang I and Wei M-H 2012 Electrical, morphological, and electromagnetic interference shielding properties of silver nanowires and nanoparticles conductive composites *Mater. Chem. Phys.* **136** 334–40
[7] Della Gaspera E, Tucker R, Star K, Lan E H, Ju Y S and Dunn B 2013 Copper-based conductive composites with tailored thermal expansion *ACS Appl. Mater. Interfaces* **5** 10966–74
[8] Klos M A H, González-García L and Kraus T 2024 Mechanically robust, inkjet-printable polymer nanocomposites with hybrid gold nanoparticles and metal-like conductivity *ACS Appl. Mater. Interfaces* **16** 31576–85
[9] Araki T, Nogi M, Suganuma K, Kogure M and Kirihara O 2011 Printable and stretchable conductive wirings comprising silver flakes and elastomers *IEEE Electron Device Lett.* **32** 1424–6
[10] Zhang L, Schmidt D S, González-García L and Kraus T 2022 Microscopic softening mechanisms of an ionic liquid additive in an electrically conductive carbon-silicone composite *Adv. Mater. Technol.* **7** 2101700
[11] Shin M K, Oh J, Lima M, Kozlov M E, Kim S J and Baughman R H 2010 Elastomeric conductive composites based on carbon nanotube forests *Adv. Mater.* **22** 2663–7
[12] Tarhini A, Tehrani-Bagha A, Kazan M and Grady B 2021 The effect of graphene flake size on the properties of graphene-based polymer composite films *J. Appl. Polym. Sci.* **138** 49821
[13] Biccai S, Boland C S, O'Driscoll D P, Harvey A, Gabbett C, O'Suilleabhain D R, Griffin A J, Li Z, Young R J and Coleman J N 2019 Negative gauge factor piezoresistive composites based on polymers filled with $MoS_2$ nanosheets *ACS Nano* **13** 6845–55
[14] Ma C, Ma M-G, Si C, Ji X-X and Wan P 2021 Flexible MXene-based composites for wearable devices *Adv. Funct. Mater.* **31** 2009524

[15] Lux F 1993 Models proposed to explain the electrical conductivity of mixtures made of conductive and insulating materials *J. Mater. Sci.* **28** 285–301
[16] Masouras K, Silikas N and Watts D C 2008 Correlation of filler content and elastic properties of resin-composites *Dent. Mater.* **24** 932–9
[17] Ervina J, Mariatti M and Hamdan S 2016 Effect of filler loading on the tensile properties of multi-walled carbon nanotube and graphene nanopowder filled epoxy composites *Proc. Chem.* **19** 897–905
[18] Li J, Ma P C, Chow W S, To C K, Tang B Z and Kim J-K 2007 Correlations between percolation threshold, dispersion state, and aspect ratio of carbon nanotubes *Adv. Funct. Mater.* **17** 3207–15
[19] Coupette F and Schilling T 2023 A universally applicable approach to connectivity percolation (arXiv:2308.16757)
[20] Nan C-W, Shen Y and Ma J 2010 Physical properties of composites near percolation *Annu. Rev. Mater. Res.* **40** 131–51
[21] Schueler R, Petermann J, Schulte K and Wentzel H-P 1997 Agglomeration and electrical percolation behavior of carbon black dispersed in epoxy resin *J. Appl. Polym. Sci.* **63** 1741–6
[22] Sumita M, Sakata K, Asai S, Miyasaka K and Nakagawa H 1991 Dispersion of fillers and the electrical conductivity of polymer blends filled with carbon black *Polym. Bull.* **25** 265–71
[23] Li Y, Wang S, Zhang Y and Zhang Y 2006 Carbon black-filled immiscible polypropylene/epoxy blends *J. Appl. Polym. Sci.* **99** 461–71
[24] Topcu G, Arenas D R, McNally T and Becer C R 2023 Microphase separation assisted reduction in the percolation threshold of MWCNT/block polymer composites *Soft Matter* **19** 1109–14
[25] Pang H, Xu L, Yan D-X and Li Z-M 2014 Conductive polymer composites with segregated structures *Prog. Polym. Sci.* **39** 1908–33
[26] Chen J, Shi Y-Y, Yang J-H, Zhang N, Huang T, Chen C, Wang Y and Zhou Z-W 2012 A simple strategy to achieve very low percolation threshold via the selective distribution of carbon nanotubes at the interface of polymer blends *J. Mater. Chem.* **22** 22398–404
[27] Bao H-D, Guo Z-X and Yu J 2008 Effect of electrically inert particulate filler on electrical resistivity of polymer/multi-walled carbon nanotube composites *Polymer* **49** 3826–31
[28] Prabhakar O P and Sahu R K 2023 Effects of soft and hard fillers on electromechanical properties and performance of polydimethylsiloxane elastomer for actuator applications *J. Appl. Polym. Sci.* **140** e54434
[29] Schmidt D S, Kraus T and González-García L 2024 Electrofluids with tailored rheoelectrical properties: liquid composites with tunable network structures as stretchable conductors *ACS Appl. Mater. Interfaces* **16** 43942–50
[30] McClements D J 2004 *Food Emulsions: Principles, Practices, and Techniques* (CRC Press)
[31] Koos E 2014 Capillary suspensions: particle networks formed through the capillary force *Curr. Opin. Colloid Interface Sci.* **19** 575–84
[32] Bhagavathi Kandy S, Simon G P, Cheng W, Zank J, Joshi K, Gala D and Bhattacharyya A R 2018 Effect of incorporation of multi-walled carbon nanotubes on the microstructure and flow behavior of highly concentrated emulsions *ACS Omega* **3** 13584–97
[33] Mazurek P, Hvilsted S and Skov A 2016 Green silicone elastomer obtained from a counterintuitively stable mixture of glycerol and PDMS *Polymer* **87** 1–7
[34] Dapčević Hadnađev T, Dokić P, Krstonošić V and Hadnađev M 2013 Influence of oil phase concentration on droplet size distribution and stability of oil-in-water emulsions *Eur. J. Lipid Sci. Technol.* **115** 313–21
[35] Sullivan A P and Kilpatrick P K 2002 The effects of inorganic solid particles on water and crude oil emulsion stability *Ind. Eng. Chem. Res.* **41** 3389–404
[36] de Souza T A, Scheer A, Khalil M C, Yamamoto C I and Luz L F D L 2012 Emulsion inversion using solid particles *J. Pet. Sci. Eng.* **96** 49–57
[37] Pal R 2011 Rheology of simple and multiple emulsions *Curr. Opin. Colloid Interface Sci.* **16** 41–60
[38] Macosko C W 1994 *Rheology principles Measurements and Applications* (Wiley)
[39] Shi S, Wang Y, Liu Y and Wang L 2018 A new method for calculating the viscosity of W/O and O/W emulsion *J. Pet. Sci. Eng.* **171** 928–37
[40] Bullard J W, Pauli A T, Garboczi E J and Martys N S 2009 A comparison of viscosity–concentration relationships for emulsions *J. Colloid Interface Sci.* **330** 186–93
[41] Mezger T G 2012 *The Rheology Handbook: Vincentz Network Hannover* (Vincentz Network)
[42] Lago-Garrido S, Schmidt D S, Martín-Alfonso M J and González-García L 2025 Multi-walled carbon nanotubes suspensions as liquid conductors: electrical and mechanical network interplay *Adv. Electron. Mater.* **11** 2400917
[43] Jiang Y, Cui Y, Li Y, Liu Z, Ness C and Seto R 2025 Filled colloidal gel rheology: strengthening, stiffening, and tunability *J. Rheol.* **69** 35–44
[44] Lee J H, Gwon S and Shin M 2021 Effect of filler particle characteristics on yield stress and viscosity of fresh sulfur composites *J. Mater. Res. Technol.* **12** 2138–52
[45] Zhou Z, Solomon M J, Scales P J and Boger D V 1999 The yield stress of concentrated flocculated suspensions of size distributed particles *J. Rheol.* **43** 651–71
[46] Hyun K, Kim S H, Ahn K H and Lee S J 2002 Large amplitude oscillatory shear as a way to classify the complex fluids *J. Non-Newton. Fluid Mech.* **107** 51–65
[47] Haridas H and Kontopoulou M 2023 Effect of specific surface area on the rheological properties of graphene nanoplatelet/poly (ethylene oxide) composites *J. Rheol.* **67** 601–19
[48] Zhang A, Zhu C, Pan D and Lin Y 2021 Study on strain stiffening of non-colloidal suspension in oscillating shear by a subsequent steady shear test *Colloids Surf. A* **618** 126401
[49] Kim H, Esser-Kahn A P, Rowan S J and Jaeger H M 2023 Stress-activated friction in sheared suspensions probed with piezoelectric nanoparticles *Proc. Natl Acad. Sci.* **120** e2310088120
[50] Seto R, Mari R, Morris J F and Denn M M 2013 Discontinuous shear thickening of frictional hard-sphere suspensions *Phys. Rev. Lett.* **111** 218301
[51] Hermes M and Clegg P S 2013 Yielding and flow of concentrated Pickering emulsions *Soft Matter* **9** 7568–75
[52] Hong J S, Kong H J, Hyun K, Bergfreund J, Fischer P and Ahn K H 2019 Rheological analysis of oil–water emulsions stabilized with clay particles by LAOS and interfacial shear moduli measurements *Rheol Acta.* **58** 453–66
[53] Mudeme S, Masalova I and Haldenwang R 2010 Kinetics of emulsification and rheological properties of highly concentrated explosive emulsions *Chem. Eng. Process.* **49** 468–75
[54] Kim H, Ahn K H and Lee S J 2017 Conductive poly (high internal phase emulsion) foams incorporated with polydopamine-coated carbon nanotubes *Polymer* **110** 187–95

[55] Princen H and Kiss A 1986 Rheology of foams and highly concentrated emulsions: III. Static shear modulus *J. Colloid Interface Sci.* **112** 427–37
[56] Malkin A Y, Masalova I, Slatter P and Wilson K 2004 Effect of droplet size on the rheological properties of highly-concentrated w/o emulsions *Rheol Acta.* **43** 584–91
[57] Lacasse M-D, Grest G S, Levine D, Mason T and Weitz D 1996 Model for the elasticity of compressed emulsions *Phys. Rev. Lett.* **76** 3448
[58] Masalova I and Malkin A Y 2007 Peculiarities of rheological properties and flow of highly concentrated emulsions: the role of concentration and droplet size *Colloid J.* **69** 185–97
[59] Mougel J, Alvarez O, Baravian C, Caton F, Marchal P, Stébé M-J and Choplin L 2006 Aging of an unstable w/o gel emulsion with a nonionic surfactant *Rheol. Acta.* **45** 555–60
[60] Hautz N and González-García L 2025 Direct ink writing of carbon-based electrofluids for soft electrical component manufacturing *Adv. Mater. Technol.* **10** e02012
[61] Peralta-Martínez M V, Arriola-Medellín A, Manzanares-Papayanopoulos E, Sánchez-Sánchez R and Palacios-Lozano E M 2004 Influence of the speed mixing-on viscosity and droplet size of oil in water emulsions *Petrol. Sci. Technol.* **22** 1035–43
[62] Sharu B, Simon G P, Cheng W, Zank J and Bhattacharyya A R 2017 Development of microstructure and evolution of rheological characteristics of a highly concentrated emulsion during emulsification *Colloids Surf. A* **532** 342–50
[63] Arganda-Carreras I, Kaynig V, Rueden C, Eliceiri K W, Schindelin J, Cardona A and Sebastian Seung H 2017 Trainable Weka Segmentation: a machine learning tool for microscopy pixel classification *Bioinformatics* **33** 2424–6